Design and Construction of Supramolecular Nanobeacons for Enzyme Detection

Lye Lin Lock, Andrew G. Cheetham, Pengcheng Zhang, and Honggang Cui*

Department of Chemical and Biomolecular Engineering, and Institute for NanoBioTechnology, The Johns Hopkins University, 3400 N. Charles Street, Baltimore, Maryland 21218, United States

ABSTRACT Molecular beacons are typically water-soluble molecules that can convert specific chemical reactions or binding events into measurable optical signals, providing a noninvasive means to help understand cellular and subcellular activities at the molecular level. However, the soluble form of the current molecular beacon design often leads to their poor stability and facile degradation by nonspecific enzymes, and as a result, this undesired activation could give rise to false signals and thus poses a limitation for accurate detection of enzymatic activities. Here we report a proof-of-concept design and synthesis of a new type of supramolecular nanobeacon that is resistant to nonspecific enzymatic degradation in the self-assembled state but can be effectively cleaved by the target enzyme in the monomeric form. Our results show that the nanobeacon with a GFLG peptide linker could serve as an indicator for the presence of a lysosomal enzyme, cathepsin B.

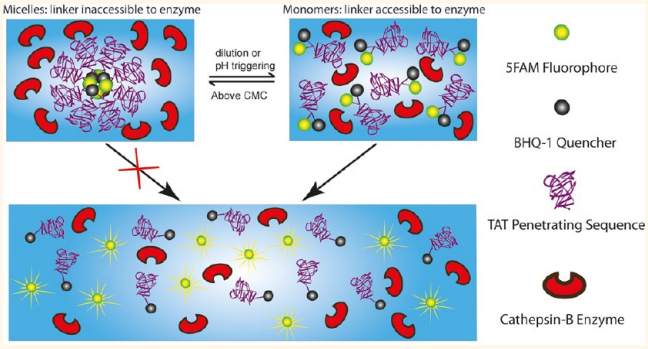

KEYWORDS: molecular assembly · peptides · enzyme detection · supramolecular nanostructures · cathepsin B · cancer

Real-time detection of the location and expression level of enzymes within living cells offers important information on many important cellular and subcellular events and thus provides unique opportunities for the development of new strategies for tumor diagnosis and cancer therapeutics.[1−4] The overexpression and relative abundance of certain proteases in cancers, such as cathepsins and matrix metalloproteases (MMPs), provide attractive targets for tumor screening.[1−3,5] In the design of polymer−drug conjugates with peptide linkers, enzymatic cleavage is an important step toward the release of bioactive anticancer drugs, with the release rate being a function of active enzyme concentration.[6−8] Recently, there is also a rapidly growing interest in the development of enzymatically responsive materials.[9−20] Therefore, it is important and necessary to precisely detect the activities or expression levels of enzymes of interest.

The advent and development of activatable molecular probes, such as molecular beacons that contain a fluorophore and quencher pair, have enabled possibilities for the highly sensitive detection of DNA/RNA through the conversion of specific binding events into detectable fluorescence signals.[21−23] Very recently, molecular beacons with proteolytically degradable peptide linkers have been devised for protease detection and other applications.[2,17,24−28] However, since the linkers that are designed to activate molecular beacons are typically exposed to the physiological environment, their poor stability and facile degradation by nonspecific enzymes often give rise to an undesired false signal and thus pose a major limitation for accurate detection of enzymatic activities.

To develop molecular probes immune to undesired degradation, we report here a generic design platform of a new type of self-assembling supramolecular nanobeacon (NB) with a well-defined size and surface chemistry for protease detection. In contrast to *soluble* molecular beacons, the NB molecules are specifically designed to self-assemble into core−shell micelles, with the enzyme-sensitive design feature being deeply embedded within the micellar core and thus inaccessible

* Address correspondence to hcui6@jhu.edu.

Received for review January 15, 2013 and accepted May 13, 2013.

Published online May 17, 2013
10.1021/nn400218a

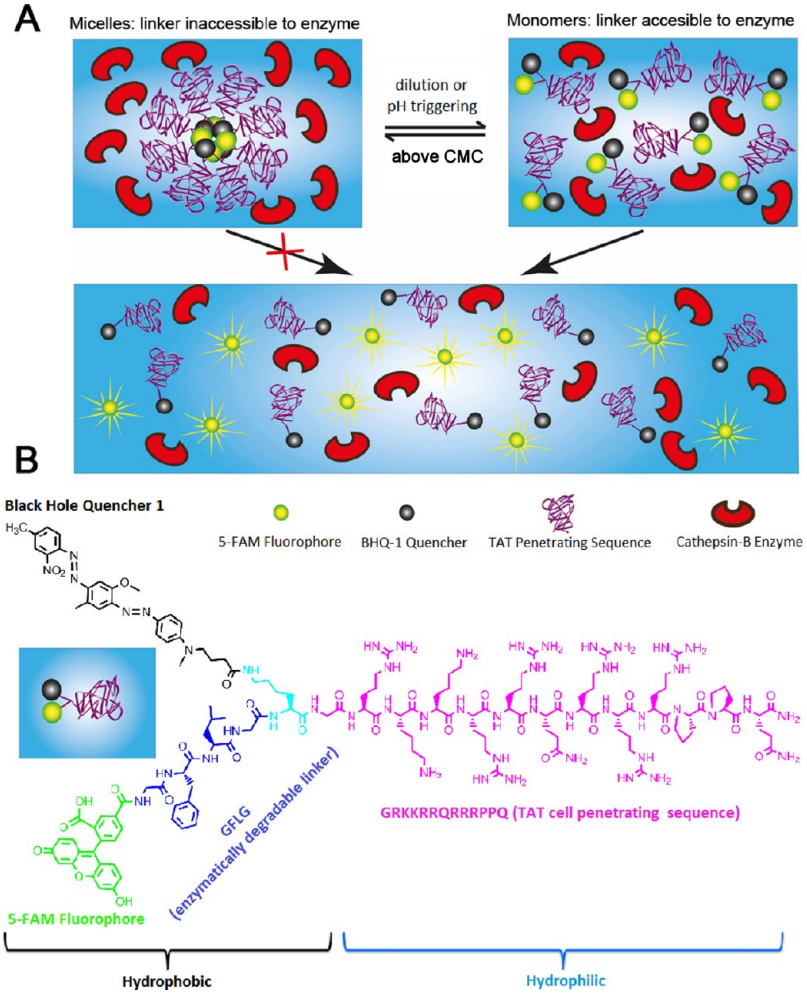

Figure 1. Schematic illustration of the expected cleavage and detection mechanism (A) and molecular structure of the designed nanobeacon molecule TFB (B). In the self-assembled state, the enzyme-sensitive linker is deeply buried in the micellar core, while in the monomeric form, the NB molecules become accessible for enzymatic cleavage. The designed molecule exists in the self-assembled NB form above its critical micellization concentration (CMC). The transition from NB micelles to monomeric form can be achieved either by dilution or by pH triggering.

to the enzyme (Figure 1A). Only in the monomeric form can these NB molecules be cleaved by the target enzyme to generate fluorescence signals.

RESULTS AND DISCUSSION

Molecular Design. The core concept of the design is to construct an amphiphilic NB molecule having the potential to self-assemble into nano-objects under physiological conditions. This amphiphilicity is achieved by conjugating a hydrophobic quencher and a dye onto a hydrophilic peptide. The concept of attaining amphiphilicity by means of conjugating two or more small-molecular chemical moieties with distinct solvent selectivity has been used to successfully construct peptide amphiphiles,[29−33] peptide nucleic acid amphiphiles,[34] and amphiphilic molecules with π-conjugated segments.[35−37] Figure 1B shows the chemical structure of the proof-of-concept NB molecule studied in this paper. First of all, the hydrophobic units are composed of a black hole quencher, BHQ-1, and a green dye, 5-carboxyfluorescein (5-FAM). 5-FAM was chosen on the basis of its exceptionally high quantum yield in the visible light region. The BHQ-1 segment with broad absorption between 400 and 650 nm (major absorption between 480 and 580 nm) will, when placed in close proximity to 5-FAM, quench the 5-FAM fluorescence without generating fluorescence of its own, thereby offering a high signal-to-noise ratio. Second, an HIV-1-derived cell penetrating peptide, Tat_{48-60},[38] with positively charged arginine and lysine amino acids, was incorporated as the hydrophilic segment to allow effective penetration of the cell membrane. The weakly basic nature of the arginine and lysine residues allows for the design of pH-responsive supramolecular nanobeacons. Finally, the key and most critical component is the cleavable linker that bridges 5-FAM and the lysine N-terminus. The peptide tetramer of -Gly-Phe-Leu-Gly- (GFLG), first identified by Kopecek, Duncan, and co-workers,[6,8] can be effectively cleaved by cathepsin B (CatB), a lysosomal protease involved in

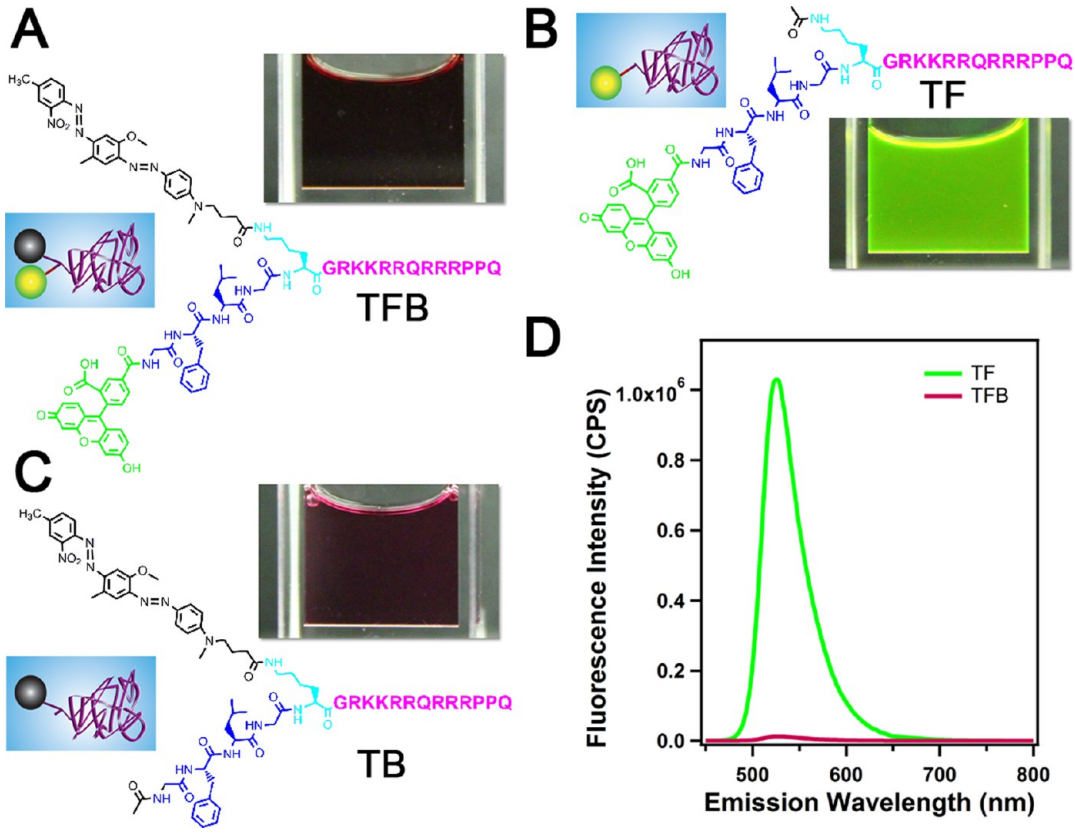

Figure 2. Photographs of 200 μM aqueous solutions of TFB (A), TF (B), and TB (C) and their respective molecular structures. The effective quenching of the 5-FAM fluorophore by the BHQ-1 segment is reflected in the dramatic color change from bright green (B) to dark red (A). (D) 5-FAM fluorescence measurements of 1 μM TF and 1 μM TFB aqueous solutions.

cellular protein turnover and degradation. We chose CatB because it plays important roles in tumor growth and progression and serves as a potential marker for tumor screening.[3,5,39−41] CatB has also attracted considerable interest as the target enzyme in the design of many polymer−drug conjugates.[6−8]

Quenching Effect. We synthesized two control molecules, TF (Figure 2B) and TB (Figure 2C), to assist in better understanding the quenching effect and self-assembly behaviors of the TFB NB molecule (S1, S2 in the Supporting Information (SI)). The effective quenching of the 5-FAM fluorophore by BHQ-1 in the NB molecule can be inferred by a change in solution color between three molecules (Figure 2A−C). At a concentration of 200 μM, the aqueous solution of the TF conjugate appears bright green, owing to the 5-FAM fluorescence around 520 nm (Figure 2B). In contrast, the aqueous solution of 200 μM TB displays a dark red color (Figure 2C) due to the absorption in the visible light region between 400 and 650 nm. The dark red color of a 200 μM TFB solution (Figure 2A), similar to that of a TB solution but distinct from that of a TF solution, strongly suggests an effective quenching of 5-FAM fluorescence. This effective quenching was further supported by the measurements of the fluorescence of the 5-FAM chromophore. It was found that the 5-FAM fluorescence intensity of a 1 μM TFB solution drops more than 80 times relative to that of a TF solution of the same molar concentration (Figure 2D), implying a greater than 98% efficiency of 5-FAM fluorescence resonance energy transfer within the designed NB molecule.

Self-Assembly and Characterization. Self-assembly was initiated by dissolution of the molecule into either Milli-Q water or phosphate-buffered saline (PBS). Transmission electron microscopy (TEM) studies showed that all three molecules, TFB, TF, and TB, self-assemble into spherical micelles under physiological conditions, with sizes of 11.1 $\pm$ 1.2, 18.4 $\pm$ 3.7, and 13.1 $\pm$ 1.0 nm, respectively (Figure 3A−D and S3 in the SI). A representative TEM image from a 1 $\times$ PBS solution of 200 μM TFB is shown in Figure 3A, revealing dominant nanoparticles with a uniform size of approximately 11 nm. In this image, the nanoparticles appear brighter than the background due to the use of uranyl acetate as a negative staining agent, which deposits more on the background and thus reverses the image contrast. The size and shape of these nanobeacons were further confirmed using cryogenic TEM imaging techniques (Figure 3B), which involve no staining but direct imaging of the liquid sample solution. Since the Tat peptide is rich in arginines and lysines, one would expect that the self-assembly behaviors of all three studied molecules are pH-dependent. Indeed, we found that TB can self-assemble into supramolecular

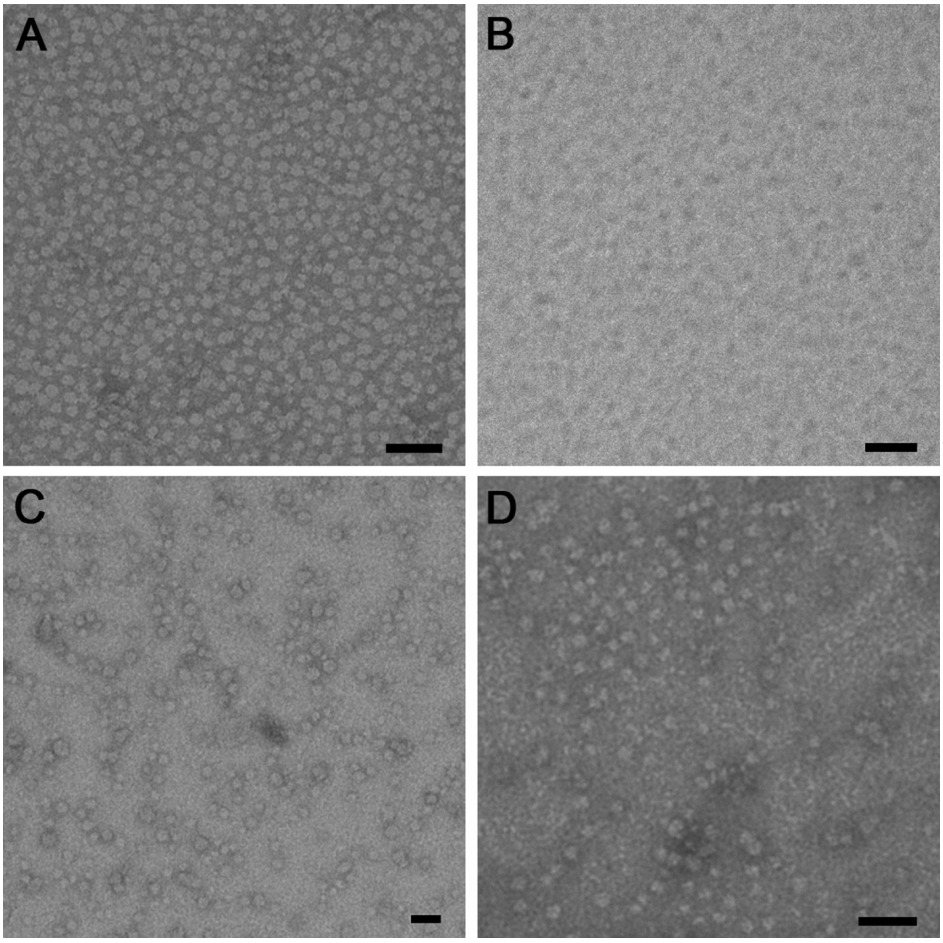

Figure 3. TEM (A) and cryo-TEM (B) images of 200 μM TFB in 1× PBS solutions reveal self-assembled nanoparticles of a uniform size (11.1 ± 1.2 nm). TEM images of nanoparticles formed by self-assembly of 400 μM TF (C) and TB (D) in 1× PBS solutions with sizes of 18.4 ± 3.7 and 13.1 ± 1.0 nm, respectively. TEM samples in (A), (C), and (D) were negatively stained using a 2 wt % uranyl acetate aqueous solution to enhance the image contrast. All scale bars: 50 nm.

filaments in borate buffer (pH 9.5) (S4 in the SI), in contrast to the spherical nanostructures in 1× PBS (pH 7.4). We believe that this morphological transition is driven by the reduced electrostatic repulsions among the Tat peptides as a result of the deprotonation of amine groups at higher pH.

Circular dichroism measurements show that the hydrophilic Tat sequence assumes a polyproline type II-like secondary structure under physiological conditions (S5 in the SI). The diameter of 11 nm is reasonably close to twice that of the expected molecular length of TFB. The amphiphilic nature of the TFB leads us to conclude that nanoparticles observed in Figure 3A are core–shell micelles with the 5-FAM and BHQ-1 segments composing the core. Since enzyme-catalyzed reactions often involve the formation of enzyme–substrate complexes, the fact that the –GFLG– linkers are deeply embedded within the micellar core suggests that in the assembled state the –GFLG– peptide linkers would be inaccessible to CatB for cleavage.

Enzymatic Degradation. Digestion experiments were carried out to evaluate the degradation kinetics of TFB NBs by CatB (S6 in the SI). In these experiments, CatB was first activated for 5 min at 37 °C using a reaction buffer containing 1 mM EDTA and 25 mM L-cysteine. All solutions were adjusted to pH 5.0 to ensure proper CatB function. NB from a stock solution (1 mM) was then introduced to solutions containing the desired amount of activated CatB, and the solution fluorescence was subsequently monitored.

Figure 4A shows that in the presence of only 1 μM CatB the fluorescence intensity rapidly increases with time, with an approximate 25-fold increase in the peak intensity at 520 nm within 80 min. After a sufficient time for cleavage, the solution color was observed to change from light red to light yellow (Figure 4B). The small fluorescence peak in the absence of CatB arises from incomplete quenching of 5-FAM, and its intensity did not change over time, suggesting that the TFB molecules are rather stable under the experimental conditions. It is also important to note that when MMP-2 was added to the TFB NB solution, no noticeable cleavage reaction was observed throughout the course of 4 h incubation (S7 in the SI).

In order to correlate the fluorescence intensity to the enzyme activity and also to understand the enzyme cleavage efficiency on the studied NB molecule,

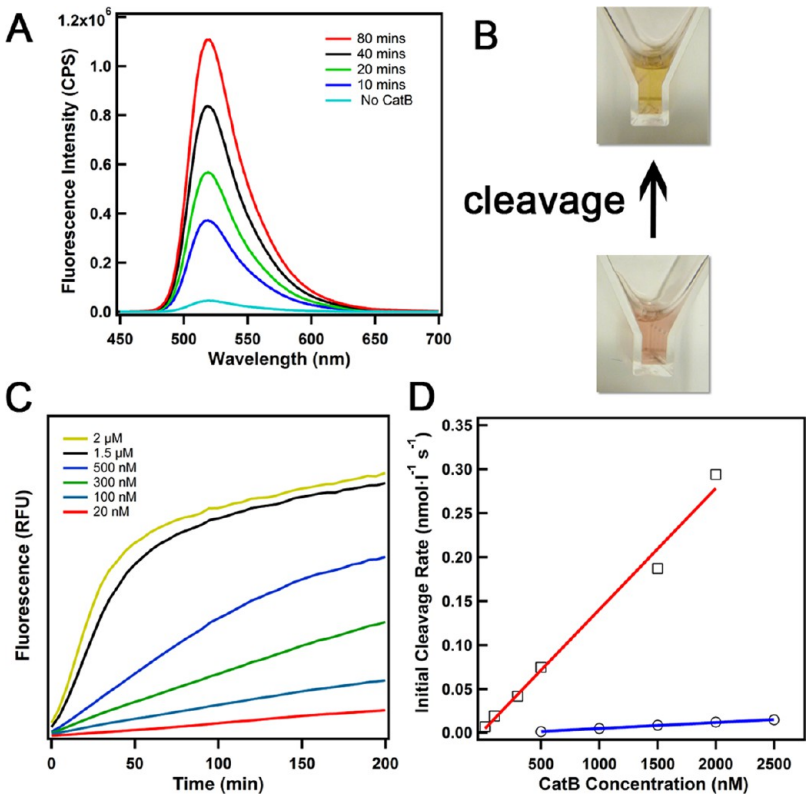

Figure 4. Fluorescence monitoring of the degradation process of NBs by CatB. (A) Time-course fluorescence measurements of a 3 μM TFB 1× PBS solution in the presence of 1 μM CatB; (B) photographs of NB solutions before and after CatB cleavage; (C) fluorescent measurement of 1 μM TFB PBS solutions in the presence of various concentrations of CatB; (D) plot of initial rate of 5-FAM cleavage *versus* CatB concentration (square, 1 μM TFB; circle, 50 μM TFB). The red and blue lines show a linear fit for the obtained data.

we performed a series of experiments on 1 μM TFB solutions while varying the amount of CatB added. The 1 μM concentration is far below the critical micellization concentration (CMC) of TFB at pH 5, which was determined to be around 30 μM using a surface tension measurement method (S8 in the SI). Figure 4C clearly reveals that an increase in CatB concentration leads to faster cleavage of 5-FAM from TFB. It is also evident that concentrations of CatB as low as 20 nM can effectively cleave the peptide linker, although the reaction proceeds at a much slower rate.

We found that the initial rate of cleavage scales linearly with the concentration of CatB (Figure 4D). The catalytic reaction of CatB has been reported to follow the kinetic behavior described by the Michaelis–Menten equation.[6,8] At very low substrate concentrations, the equation can be simplified as $V \cong (k_{cat})/(K_M)[E]_t[S]$, in which k_{cat} is the first-order rate constant, $[E]_t$ is the total enzyme concentration, [S] is the substrate (TFB, in the case reported here) concentration, and K_M is the Michaelis–Menten constant (S9 in the SI). In the particular case reported herein (–GFLG– linker cleavage by CatB), the K_M has been reported to be on the scale of mM,[6,8] a value much higher than the 1 μM TFB concentration. The ratio of k_{cat}/K_M provides a direct measure of enzyme efficiency and specificity. The plot in Figure 4D is in good agreement with this equation, as the initial cleavage rate is indeed linear with respect to the CatB concentration. The initial reaction rates, V_0, were obtained from the linear region at the very beginning of the curves presented in Figure 4C. k_{cat}/K_M was calculated using this simplified Michaelis–Menten equation and was found to be approximately 137 $(mol/L)^{-1}$ s^{-1} (S9 in the SI). This value shows a reasonable degradation efficiency of the –GFLG– linker to CatB digestion. This finding also implies that quantitative detection of CatB in live cells is possible once accurate measurements of the initial reaction rate and the local concentration of the delivered NBs can be obtained.

We performed further experiments on a series of TFB solutions of different concentrations with a fixed CatB concentration (S10 in the SI). We found that the initial cleavage rate first increased with the increase of TFB concentration from 50 nM to 1 μM, as expected according to the Michaelis–Menten equation, but then started to drop after 3 μM. We attribute this drop in cleavage rate to the formation of dimers, trimers, or other TFB molecular clusters that prevent the NB from being effectively cleaved by CatB. In order to gain a better understanding of the degradation kinetics of TFB micelles, we carried out experiments on a 50 μM TFB solution, a concentration above the CMC (~30 μM). As expected, the cleavage reaction was found to proceed much more slowly, and the k_{cat}/K_M was calculated

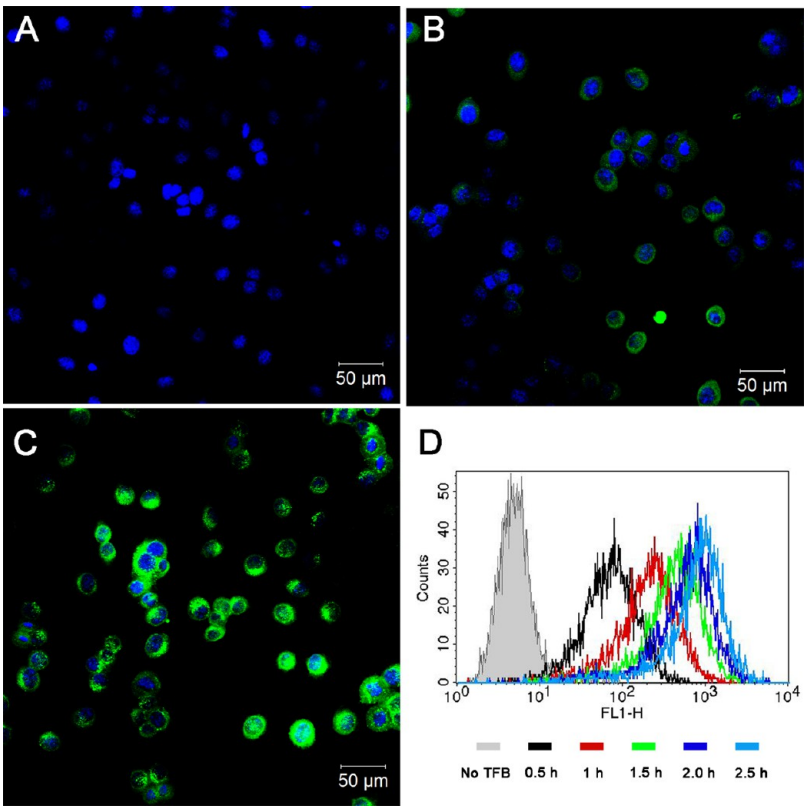

Figure 5. Time-dependent fluorescence of NB molecules inside MCF-7 human breast cancer cells. Fluorescence images of cells after 0 h (A), 0.5 h (B), and 1.5 h (C) exposure to TFB NB show increased 5-FAM fluorescence with time. The cell nuclei were stained with the blue dye Hoechst 33342. (D) Flow cytometry confirms the increased fluorescence intensity with time inside live MCF-7 cells.

to be around 0.135 $(mol/L)^{-1}\ s^{-1}$ (Figures 4D and S9 in the SI), a value almost 3 orders of magnitude lower than that of CatB cleavage on the TFB monomers. Since TFB predominantly exists in aggregates above the CMC, these results clearly suggest that the −GFLG− peptide linker is inaccessible for effective CatB cleavage and, thus, provide evidence for the expected cleavage mechanism presented in Figure 1A.

Cancer Cell Imaging. To assess the possibility of using the designed NB for detection of CatB activities in cells, MCF-7 human breast cancer cells were incubated with 5 μM TFB at 37 °C in cell media, and fluorescence images on the basis of 5-FAM emission were taken at different time points (0, 0.5, and 1.5 h) (S11 in the SI). Figure 5A−C reveals increased 5-FAM fluorescence intensity inside the MCF-7 cells with increased incubation time. Since intact TFB molecules remain dark and are not fluorescent, this result reveals that the NB molecule not only is capable of entering the cells but can also be effectively activated within cells to generate green fluorescence.

To confirm the observed 5-FAM fluorescence does not stem from potential artifacts associated with cell fixation, we used flow cytometry to investigate the time-dependent fluorescence in live cells (Figure 5D). These results are consistent with the fluorescent imaging data. The continuous increase in fluorescence intensity with prolonged incubation time suggests effective cellular uptake of NB molecules. We speculate this effective internalization might be a combined effect of using the Tat cell penetrating peptide with the amphiphilic design of the NB molecule. We also found that the geo-mean fluorescence intensity increases linearly with time (Figure S11 of S11 in the SI); however, this linear correlation should be interpreted with caution and cannot be used to directly quantify CatB within cells because it is not clear whether the cellular uptake or the CatB cleavage reaction is the rate-limiting step and whether other factors such as pH or ionic strength also contribute to the measured florescence intensity.

To evaluate if the internalized TFB NBs were indeed cleaved by the CatB enzyme, a CatB inhibitor (CA-074 Me) was used to suppress the CatB activity in cells. Both of our fluorescence and flow cytometery experiments reveal that the 5-FAM fluorescence intensity is significantly reduced in the presence of the inhibitor (Figures S12 and S13 of S11 in the SI). We also performed experiments to show that the inhibitor does not interfere with the cellular uptake of the TFB and the viability of the studied cells (Figures S14 and S15 of S11 in the SI). These experiments clearly suggest the specific cleavage of TFB NB by CatB. Co-localization experiments were also performed to verify the locations from where the 5-FAM fluorescence was generated. Lysosomes of MCF-7 cells were labeled with Lysotracker Red.

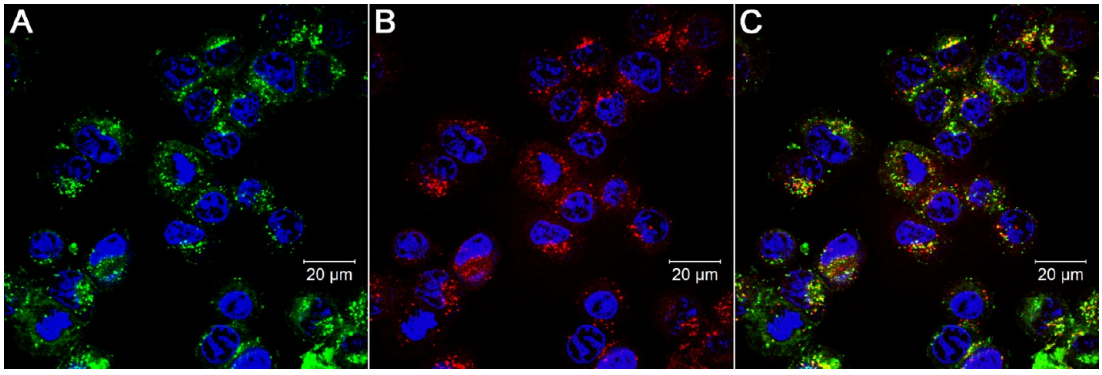

Figure 6. Confocal fluorescence images of MCF-7 cells after 2.5 h incubation with NB molecules show co-localization of the fluorescence signal of 5-FAM with that of the Lysotracker Red. (A) Image of 5-FAM fluorescence. (B) Image of Lysotracker Red fluorescence and (C) merged image of (A) and (B). The cell nuclei were stained with the blue dye Hoechst 33342.

As shown in Figure 6, the merged fluorescence image (Figure 6C) shows almost complete overlap of the 5-FAM green fluorescence with the Lysotracker Red fluorescence, indicating the 5-FAM fluorescence arises from lysosomes where CatB is expected to reside.

For the TFB concentrations used in all these studies, cell viability tests show the TFB NB has little toxicity to MCF-7 cells during the incubation (Figure S16 of S11 in the SI). However, for concentrations higher than 30 μM we found that our designed NB started to show toxicity to cultured cells and that most cells died after incubating the beacon for only a few minutes, most likely due to the positive charge nature of the Tat peptide. Therefore, the future design must take into consideration the potential toxicity of positively charged cell penetrating peptides at high concentrations.

In a brief summary, these results reveal the possibility of using TFB NB for cancer cell imaging: under physiological conditions and above their CMCs, the designed NB molecules self-assemble into spherical micelles with the cleavable linker buried within the core. Upon accumulation in the tumor microenvironment or entering the lysosomes, which are known to have an acidic environment, the NBs can be expected to gradually dissociate to individual molecules due to dilution or/and pH triggering, thereby exposing the cleavable linker to the target enzyme. Eventually, in the presence of CatB, 5-FAM will be released and its fluorescence can be used as an indicator for the presence of CatB.

Conclusion and Future Prospects. In this work, we demonstrate a generic design of a new type of supramolecular nanobeacon by incorporating a fluorophore, a quencher, and a hydrophilic cell penetrating peptide into one amphiphilic molecule. Our results clearly reveal the difference in CatB degradation kinetics between TFB molecules and supramolecular nanostructures and demonstrate the potential for possible cancer cell imaging. However, there are still many challenges ahead for the development of supramolecular nanobeacons suitable for *in vivo* studies. First and foremost, the CMC value must be lowered to the nanomolar range to construct stable supramolecuar beacons during the circulation. The CMC value of our current design is around 30 μM, and at this concentration or above the TFB molecule shows great cytotoxicity. As a result, it would not be possible to maintain such a high concentration in plasma due to this observed toxicity. Second, a greater challenge is the controlled dissociation of supramolecular beacons into monomeric form. New features must be included in the design such that self-assembled nanobeacons can undergo a specific transition into monomeric form upon reaching the targeted sites. The dilution and pH triggering mechanisms of the current system, although suitable for imaging purposes, could present a limitation or hurdle for quantification of enzymatic activities. Third, other important parameters must also be considered, including the emission range of the chosen dye (near-infrared dye is preferred for *in vivo* studies), the potential effects of pH and ionic strengths on the fluorescence intensity, cellular uptake mechanisms associated with different cell types, the rate-limiting steps for the cleavage reactions, and the inclusion of a second type of molecular probe of different modalities for deep tissue tracking. Despite these intimidating challenges, we believe that the facile tunability of supramolecular nanomaterials in size, shape, and surface chemistry offers new opportunities for the development of enzyme sensors for the imaging and diagnosis of cancer cells.

METHODS

Molecular Synthesis. In brief, the Tat sequence and the peptide linker (Fmoc-GFLGK(Mtt)GRKKRRQRRRPPQ-Rink) of the TFB molecule were first synthesized on an automatic peptide synthesizer (details of synthesis can be found in the SI) using standard 9-fluorenylmethoxycarbonyl (Fmoc) solid phase synthesis protocols. After removal of the Fmoc protecting group, 5-FAM was manually coupled at the peptide N-terminus. Next,

black hole quencher-1 (BHQ-1) was incorporated onto the lysine ε-amine, following removal of the Mtt protecting group for lysine side chains. The completed peptide was cleaved from the Rink Amide resin using a mixture of TFA/TIS/H_2O. The two control molecules, TF and TB, were synthesized by using acetic anhydride to replace the BHQ-1 and the 5-FAM segments with an acetyl group, following the same procedures for the synthesis of the TFB molecule. All the molecules were purified using preparative RP-HPLC, and their purity was evaluated by analytical HPLC and MALDI-ToF mass spectrometry.

Cathepsin B Degradation Experiments. The reaction buffer containing 1 mM EDTA (enzyme stabilizer) and 25 mM L-cysteine (enzyme activator) in 1× PBS solution was prepared. The solution pH was adjusted to 5.0 through the addition of 3 M HCl. The desired amount of cathepsin-B was added to the buffer solution and preincubated at 37 °C for 5 min to activate the enzyme. Stock solution was prepared by dissolving 0.6 mg of TFB molecule with 500 μL of pH 5.0 reaction buffer, yielding a TFB concentration of 0.4 mM. A 0.25 μL amount of a 0.4 mM stock solution was added to each reaction well and mixed thoroughly with the preincubated cathepsin-B solution. Cathepsin-B (bovine spleen) was purchased from EMD Chemicals (Gibbstown, NJ, USA), and it was delivered in liquid form with a stock concentration of 17 μM. Reaction kinetics was monitored using a Gemini XPS microplate reader (Molecular Devices, Sunnyvale, CA, USA). Samples were excited at 492 nm, and 5-FAM emission was measured at 520 nm with a 515 nm cutoff.

k_{cat}/K_M Calculation. The catalytic reaction of CatB has been reported to follow the kinetic behavior described by the Michaelis–Menten equation. According to the Michaelis–Menten equation, the reaction rate V can be expressed in the following form:

$$V = \frac{k_{cat}[E]_t[S]}{K_M + [S]}$$

in which k_{cat} is the first-order rate constant, $[E]_t$ is the total enzyme concentration, [S] is the substrate (TFB, in the case reported here) concentration, and K_M is the Michaelis–Menten constant. At the very low substrate concentrations reported herein ($[S] \ll K_M$), the equation can be rewritten as

$$V \cong \frac{k_{cat}}{K_M}[E]_t[S]$$

The ratio of k_{cat}/K_M provides a direct measure of enzyme efficiency and specificity.

Cell Culture. Human breast adenocarcinoma cell line MCF-7 was kindly provided by the Wirtz Lab at The Johns Hopkins University and was grown in Dulbecco's modified Eagle medium (Invitrogen) containing 10% fetal bovine serum (Invitrogen) and 1% penicillin and streptomycin (Invitrogen). The breast cancer cells were incubated at 37 °C in a humidified incubator with a 5% CO_2 atmosphere in all cell experiments.

Cytotoxicity Assay. The cytotoxicity of the TFB was evaluated on MCF-7 cells to make sure that the cells were healthy in the following experiments. Briefly, MCF-7 cells were seeded onto a 96-well plate at a density of 5×10^3 cells/well and allowed to attach overnight. The medium was replaced with fresh complete medium (as described in the cell culture protocol) containing 0, 1, 5, or 10 μM TFB and incubated for 4 h. Then, the medium was changed to fresh complete medium and incubated for another 48 h, and the cell viability was evaluated using a sulforhodamine B (SRB)-based method according to the manufacturer's protocol (TOX-6, Sigma).

Flow Cytometry Measurement. The time-dependent fluorescence increase on MCF-7 was quantified using a flow cytometer (FACSCalibur, BD). MCF-7 cells were seeded onto a 24-well plate at a density of 1×10^5 cells/well and allowed to attach overnight. The medium was replaced with fresh complete medium containing 5 μM TFB and incubated for 0.5, 1, 1.5, 2, and 2.5 h. Then, the cells were washed once with DPBS and further treated with trypsin to harvest cells from each well. Finally, MCF-7 cells were washed three times with ice-cold DPBS and immediately analyzed using a flow cytometer at the FL1 channel. The viable cells were gated according to forward scatter *versus* side scatter profile, and the data were analyzed using Cell Quest Pro software.

Confocal Imaging. The time-dependent fluorescence increase in MCF-7 cells was imaged using a confocal laser scanning microscope (CLSM, LSM 510, Zeiss) leaving the pinhole wide open. Briefly, MCF-7 cells were seeded onto a collagen (Invitrogen)-coated eight-chamber glass-bottom plate (Lab-Tek) at a density of 3×10^4 cells/well and allowed to attach overnight. The medium was replaced with fresh complete medium containing 5 μM TFB. After 0.5 and 1.5 h incubation, the cells were washed three times with DPBS and fixed with 100 μL of 4% paraformaldehyde for 10 min at 4 °C. Then, the paraformaldehyde was removed, and the cells were washed three times with DPBS. In the co-localization experiment, the cells were seeded and treated in the same manner except 100 nM Lysotracker Red (Invitrogen) and 5 μg/mL Hoechst 33342 (Invitrogen) were added to stain the lysosome and nucleus, respectively. These two dyes were added 20 min before cell fixation. Finally, 100 μL of Fluomount-G (Southernbiotech) was added, and the samples were imaged immediately using CLSM (pinhole sizes were set to obtain optical slices at 0.9 μm).

Conflict of Interest: The authors declare no competing financial interest.

Acknowledgment. The work reported here is supported by W.W. Smith Charitable Trust and the Johns Hopkins New Faculty Startup Grant. We thank the Integrated Imaging Center (IIC) at The Johns Hopkins University for TEM and cryo-TEM imaging. We also thank Dr. Ostermeier, Dr. Hristova, Dr. Konstantopoulos, Dr. Mao and Dr. Frechette for the use of the fluorescence spectrometer, CD spectropolarimeter, flow cytometer, plate reader, and surface tension measurement instrument, respectively.

Supporting Information Available: Details of molecular synthesis and characterization, TEM sample preparation and imaging, CD measurement, CMC determination, cell culture, fixation and imaging, flow cytometry measurement, and cytotoxicity experiments can be found in online supporting material. This material is available free of charge *via* the Internet at http://pubs.acs.org.

REFERENCES AND NOTES

1. Funovics, M.; Weissleder, R.; Tung, C. H. Protease Sensors for Bioimaging. *Anal. Bioanal. Chem.* **2003**, *377*, 956–963.
2. Lee, S.; Xie, J.; Chen, X. Y. Activatable Molecular Probes for Cancer Imaging. *Curr. Top. Med. Chem.* **2010**, *10*, 1135–1144.
3. Weissleder, R.; Tung, C. H.; Mahmood, U.; Bogdanov, A. *In Vivo* Imaging of Tumors with Protease-Activated Near-Infrared Fluorescent Probes. *Nat. Biotechnol.* **1999**, *17*, 375–378.
4. Whitney, M. A.; Crisp, J. L.; Nguyen, L. T.; Friedman, B.; Gross, L. A.; Steinbach, P.; Tsien, R. Y.; Nguyen, Q. T. Fluorescent Peptides Highlight Peripheral Nerves during Surgery in Mice. *Nat. Biotechnol.* **2011**, *29*, 352–U181.
5. Jedeszko, C.; Sloane, B. F. Cysteine Cathepsins in Human Cancer. *Biol. Chem.* **2004**, *385*, 1017–1027.
6. Duncan, R.; Cable, H. C.; Lloyd, J. B.; Rejmanova, P.; Kopecek, J. Polymers Containing Enzymatically Degradable Bonds.7. Design of Oligopeptide Side-Chains in Poly N-(2-Hydroxypropyl)-Methacrylamide Co-Polymers to Promote Efficient Degradation by Lysosomal-Enzymes. *Macromol. Chem. Phys.* **1983**, *184*, 1997–2008.
7. Pasut, G.; Veronese, F. M. Polymer-Drug Conjugation, Recent Achievements and General Strategies. *Prog. Polym. Sci.* **2007**, *32*, 933–961.
8. Rejmanova, P.; Kopecek, J.; Pohl, J.; Baudys, M.; Kostka, V. Polymers Containing Enzymatically Degradable Bonds 0.8. Degradation of Oligopeptide Sequences in N-(2-Hydroxypropyl)Methacrylamide Co-Polymers by Bovine Spleen Cathepsin-B. *Macromol. Chem. Phys.* **1983**, *184*, 2009–2020.
9. Galler, K. M.; Aulisa, L.; Regan, K. R.; D'Souza, R. N.; Hartgerink, J. D. Self-Assembling Multidomain Peptide Hydrogels:

Designed Susceptibility to Enzymatic Cleavage Allows Enhanced Cell Migration and Spreading. *J. Am. Chem. Soc.* **2010**, *132*, 3217–3223.
10. Gao, Y.; Shi, J.; Yuan, D.; Xu, B. Imaging Enzyme-Triggered Self-Assembly of Small Molecules inside Live Cells *Nat. Commun.* **2012**, *3*.
11. Gao, Y.; Zhao, F.; Wang, Q. G.; Zhang, Y.; Xu, B. Small Peptide Nanofibers as the Matrices of Molecular Hydrogels for Mimicking Enzymes and Enhancing the Activity of Enzymes. *Chem. Soc. Rev.* **2010**, *39*, 3425–3433.
12. Ghadiali, J. E.; Stevens, M. M. Enzyme-Responsive Nanoparticle Systems. *Adv. Mater.* **2008**, *20*, 4359–4363.
13. Giano, M. C.; Pochan, D. J.; Schneider, J. P. Controlled Biodegradation of Self-Assembling *Beta*-Hairpin Peptide Hydrogels by Proteolysis with Matrix Metalloproteinase-13. *Biomaterials* **2011**, *32*, 6471–6477.
14. Hahn, M. E.; Gianneschi, N. C. Enzyme-Directed Assembly and Manipulation of Organic Nanomaterials. *Chem. Commun.* **2011**, *47*, 11814–11821.
15. Hirst, A. R.; Roy, S.; Arora, M.; Das, A. K.; Hodson, N.; Murray, P.; Marshall, S.; Javid, N.; Sefcik, J.; Boekhoven, J.; van Esch, J. H.; Santabarbara, S.; Hunt, N. T.; Ulijn, R. V. Biocatalytic Induction of Supramolecular Order. *Nat. Chem.* **2010**, *2*, 1089–1094.
16. Levesque, S. G.; Shoichet, M. S. Synthesis of Enzyme-Degradable, Peptide-Cross-Linked Dextran Hydrogels. *Bioconjugate Chem.* **2007**, *18*, 874–885.
17. Lowe, S. B.; Dick, J. A. G.; Cohen, B. E.; Stevens, M. M. Multiplex Sensing of Protease and Kinase Enzyme Activity *via* Orthogonal Coupling of Quantum Dot Peptide Conjugates. *ACS Nano* **2012**, *6*, 851–857.
18. Lutolf, M. P.; Lauer-Fields, J. L.; Schmoekel, H. G.; Metters, A. T.; Weber, F. E.; Fields, G. B.; Hubbell, J. A. Synthetic Matrix Metalloproteinase-Sensitive Hydrogels for the Conduction of Tissue Regeneration: Engineering Cell-Invasion Characteristics. *Proc. Natl. Acad. Sci. U.S.A.* **2003**, *100*, 5413–5418.
19. Raeber, G. P.; Lutolf, M. P.; Hubbell, J. A. Molecularly Engineered PEG Hydrogels: A Novel Model System for Proteolytically Mediated Cell Migration. *Biophys. J.* **2005**, *89*, 1374–1388.
20. Williams, R. J.; Smith, A. M.; Collins, R.; Hodson, N.; Das, A. K.; Ulijn, R. V. Enzyme-Assisted Self-Assembly under Thermodynamic Control. *Nat. Nanotechnol.* **2009**, *4*, 19–24.
21. Tan, W. H.; Wang, K. M.; Drake, T. J. Molecular Beacons. *Curr. Opin. Chem. Biol.* **2004**, *8*, 547–553.
22. Tyagi, S.; Bratu, D. P.; Kramer, F. R. Multicolor Molecular Beacons for Allele Discrimination. *Nat. Biotechnol.* **1998**, *16*, 49–53.
23. Tyagi, S.; Kramer, F. R. Molecular Beacons: Probes That Fluoresce upon Hybridization. *Nat. Biotechnol.* **1996**, *14*, 303–308.
24. Chen, J.; Liu, T. W. B.; Lo, P. C.; Wilson, B. C.; Zheng, G. "Zipper" Molecular Beacons: A Generalized Strategy to Optimize the Performance of Activatable Protease Probes. *Bioconjugate Chem.* **2009**, *20*, 1836–1842.
25. Ghadiali, J. E.; Lowe, S. B.; Stevens, M. M. Quantum-Dot-Based FRET Detection of Histone Acetyltransferase Activity. *Angew. Chem., Int. Ed.* **2011**, *50*, 3417–3420.
26. Olson, E. S.; Jiang, T.; Aguilera, T. A.; Nguyen, Q. T.; Ellies, L. G.; Scadeng, M.; Tsien, R. Y. Activatable Cell Penetrating Peptides Linked to Nanoparticles as Dual Probes for *in Vivo* Fluorescence and MR Imaging of Proteases. *Proc. Natl. Acad. Sci. U.S.A.* **2010**, *107*, 4311–4316.
27. Thurley, S.; Roglin, L.; Seitz, O. Hairpin Peptide Beacon: Dual-Labeled PNA-Peptide-Hybrids for Protein Detection. *J. Am. Chem. Soc.* **2007**, *129*, 12693–12695.
28. Zheng, G.; Chen, J.; Stefflova, K.; Jarvi, M.; Li, H.; Wilson, B. C. Photodynamic Molecular Beacon as an Activatable Photosensitizer Based on Protease-Controlled Singlet Oxygen Quenching and Activation. *Proc. Natl. Acad. Sci. U.S.A.* **2007**, *104*, 8989–8994.
29. Hartgerink, J. D.; Beniash, E.; Stupp, S. I. Self-Assembly and Mineralization of Peptide-Amphiphile Nanofibers. *Science* **2001**, *294*, 1684–1688.
30. Lowik, D.; Van den Heuvel, M.; Van Hest, J. Peptide-Amphiphile Based Polydiacetylenes: Making Nanofibers of Defined Dimensions. *J. Pept. Sci.* **2010**, *16*, 36–37.
31. Paramonov, S. E.; Jun, H. W.; Hartgerink, J. D. Self-Assembly of Peptide-Amphiphile Nanofibers: The Roles of Hydrogen Bonding and Amphiphilic Packing. *J. Am. Chem. Soc.* **2006**, *128*, 7291–7298.
32. Trent, A.; Marullo, R.; Lin, B.; Black, M.; Tirrell, M. Structural Properties of Soluble Peptide Amphiphile Micelles. *Soft Matter* **2011**, *7*, 9572–9582.
33. Yu, Y. C.; Berndt, P.; Tirrell, M.; Fields, G. B. Self-Assembling Amphiphiles for Construction of Protein Molecular Architecture. *J. Am. Chem. Soc.* **1996**, *118*, 12515–12520.
34. Vernille, J. P.; Kovell, L. C.; Schneider, J. W. Peptide Nucleic Acid (PNA) Amphiphiles: Synthesis, Self-Assembly, and Duplex Stability. *Bioconjugate Chem.* **2004**, *15*, 1314–1321.
35. De Greef, T. F. A.; Smulders, M. M. J.; Wolffs, M.; Schenning, A. P. H. J.; Sijbesma, R. P.; Meijer, E. W. Supramolecular Polymerization. *Chem. Rev.* **2009**, *109*, 5687–5754.
36. Hill, J. P.; Jin, W. S.; Kosaka, A.; Fukushima, T.; Ichihara, H.; Shimomura, T.; Ito, K.; Hashizume, T.; Ishii, N.; Aida, T. Self-Assembled Hexa-Peri-Hexabenzocoronene Graphitic Nanotube. *Science* **2004**, *304*, 1481–1483.
37. Matmour, R.; De Cat, I.; George, S. J.; Adriaens, W.; Leclere, P.; Bomans, P. H. H.; Sommerdijk, N. A. J. M.; Gielen, J. C.; Christianen, P. C. M.; Heldens, J. T.; van Hest, J. C. M.; Lowik, D. W. P. M.; De Feyter, S.; Meijer, E. W.; Schenning, A. P. H. J. Oligo(*p*-phenylenevinylene)-Peptide Conjugates: Synthesis and Self-Assembly in Solution and at the Solid-Liquid Interface. *J. Am. Chem. Soc.* **2008**, *130*, 14576–14583.
38. Vives, E.; Brodin, P.; Lebleu, B. A Truncated HIV-1 Tat Protein Basic Domain Rapidly Translocates through the Plasma Membrane and Accumulates in the Cell Nucleus. *J. Biol. Chem.* **1997**, *272*, 16010–16017.
39. Eijan, A. M.; Sandes, E. O.; Riveros, M. D.; Thompson, S.; Pasik, L.; Mallagrino, H.; Celeste, F.; Casabe, A. R. High Expression of Cathepsin B in Transitional Bladder Carcinoma Correlates with Tumor Invasion. *Cancer* **2003**, *98*, 262–268.
40. Maguire, T. M.; Shering, S. G.; Duggan, C. M.; McDermott, E. W.; O'Higgins, N. J.; Duffy, M. J. High Levels of Cathepsin B Predict Poor Outcome in Patients with Breast Cancer. *Int. J. Biol. Marker.* **1998**, *13*, 139–144.
41. Reinheckel, T.; Deussing, J.; Roth, W.; Peters, C. Towards Specific Functions of Lysosomal Cysteine Peptidases: Phenotypes of Mice Deficient for Cathepsin B or Cathepsin L. *Biol. Chem.* **2001**, *382*, 735–741.